OAA Technical Memorandum ERL WPL-114

A CASE STUDY OF LAYER FINE STRUCTURE AND TURBULENCE WITHIN STABLE ELEVATED LAYERS

Wave Propagation Laboratory
Boulder, Colorado
September 1983

noaa NATIONAL OCEANIC AND ATMOSPHERIC ADMINISTRATION / Environmental Research Laboratories

NOAA Technical Memorandum ERL WPL-114

A CASE STUDY OF LAYER FINE STRUCTURE AND TURBULENCE WITHIN STABLE ELEVATED LAYERS

Earl Gossard

Cooperative Institute for Research in Environmental Sciences
University of Colorado
Boulder, Colorado

William Neff
Robert Zamora

Report Prepared for the Naval Ocean Systems Center
Under Military Interdepartmental Purchase Request
N6600182MP0008. Contract Monitor: J. H. Richter

Wave Propagation Laboratory
Boulder, Colorado
September 1983

UNITED STATES
DEPARTMENT OF COMMERCE

Malcolm Baldrige,
Secretary

NATIONAL OCEANIC AND
ATMOSPHERIC ADMINISTRATION

John V. Byrne,
Administrator

Environmental Research
Laboratories

Vernon E. Derr,
Acting Director

NOTICE

Mention of a commercial company or product does not constitute an endorsement by NOAA Environmental Research Laboratories. Use for publicity or advertising purposes of information from this publication concerning proprietary products or the tests of such products is not authorized.

CONTENTS

A CASE STUDY OF LAYER FINE STRUCTURE AND TURBULENCE WITHIN STABLE ELEVATED LAYERS

Earl Gossard

Cooperative Institute for Research in Environmental Sciences

University of Colorado/NOAA, Boulder

William Neff and Robert Zamora

NOAA/ERL/Wave Propagation Laboratory

Boulder, Colorado 80303

SUMMARY

Profiles of the wind and temperature structure within an elevated temperature inversion lying across the BAO 300 meter tower near Erie, Colorado reveal a fine structure reminiscent of the sheet and layer structure often seen in the ocean thermocline and in estuaries and lakes.

Detailed examination indicates that the profiles of wind and temperature sometimes "saturate", adjusting themselves to a critical Richardson Number just small enough to maintain turbulence; the turbulence is created by shear instability of Kelvin-Helmholtz waves. The result offers hope of sensing temperature gradients aloft remotely from ground-based radar measurements of wind, but it is shown that profiles retrieved by the integration of the gradients will be inaccurate. One possible approach to the use of such a system for meteorological purposes would be to reformulate meteoro-

meteorological problems in terms of temperature gradient, layer thickness and layer height. Another approach might be to incorporate the gradient and height information into radiometric profile retrieval processing to provide accurate integrated profiles. To be very accurate, either approach requires the fine structure in the wind profile, but the high resolution required to resolve the fine structure poses a difficult engineering problem.

INTRODUCTION

On 20 May 1981 the lower troposphere was very stably stratified near the Boulder Atmospheric Observatory (BAO), as revealed by the RAWIN sounding taken at 0644 MST shown in Fig. 1. The lowest layers, in fact, lay across the BAO 300-m tower at Erie, Colo. from 0500 to 0900 MST as shown by the radar and acoustic soundings in Figs. 2 and 3. A detailed description of the BAO facility is given by Kaimal (1978). During the period a series of profiles of atmospheric properties was obtained by running the carriage up and down the 300-m tower. Periodically the carriage was placed at a level approximately midway between two fixed levels to measure turbulent quantities, while gradient quantities were measured with accurate fixed-level sensors, Gossard et al. (1983).

A sample of the carriage operation is shown in Fig. 4. It carried two instrumented booms separated vertically by 10.3 m. Each boom was instrumented with a prop-vane anemometer, a quartz thermometer, and a platinum wire thermometer. In addition, the lower boom had a sonic anemometer and a device for measuring the temperature structure parameter, C_T^2, described by Ochs and

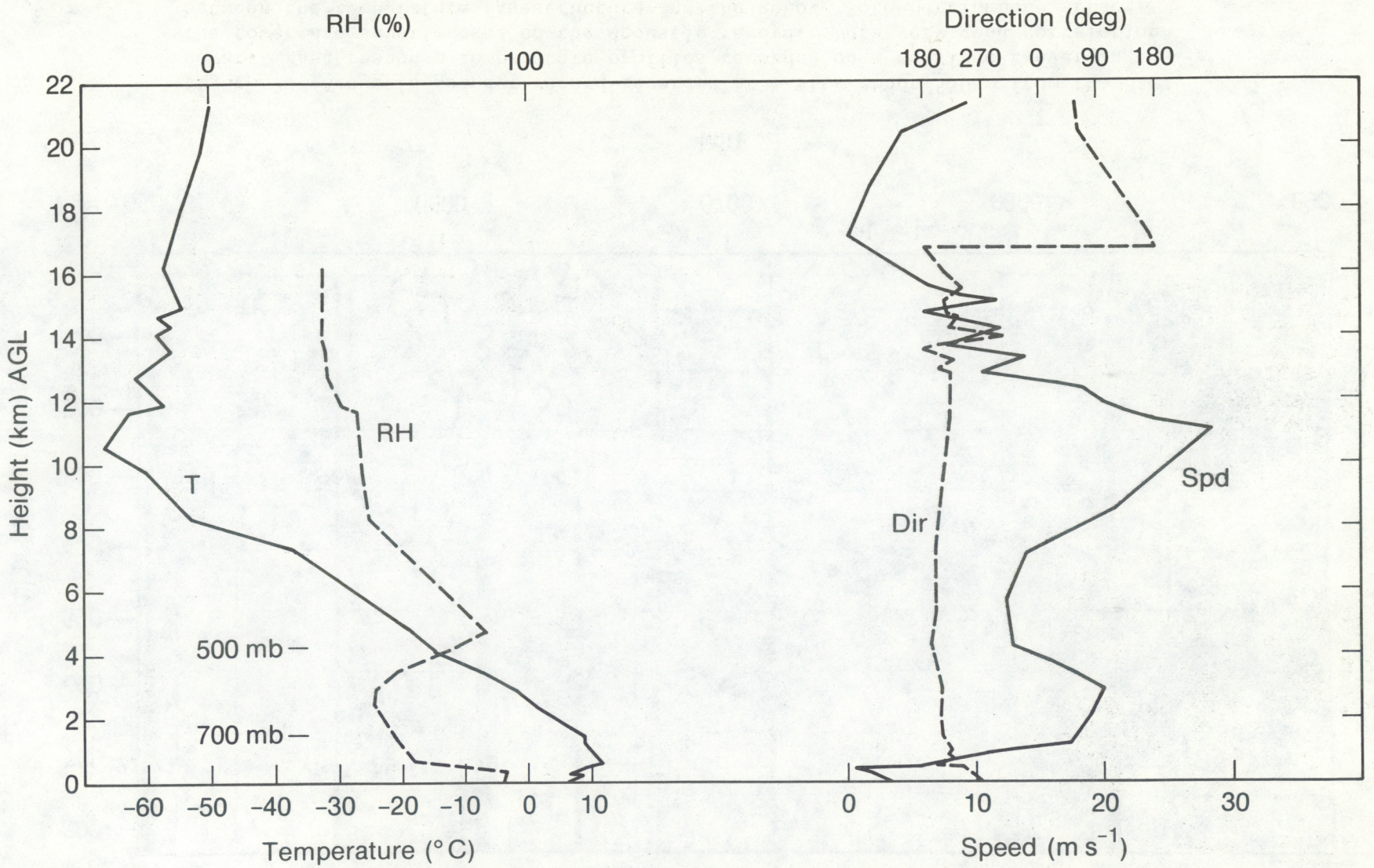

Figure 1.--RAWIN launched at 0644 from site at the BAO tower near Erie, Colorado.

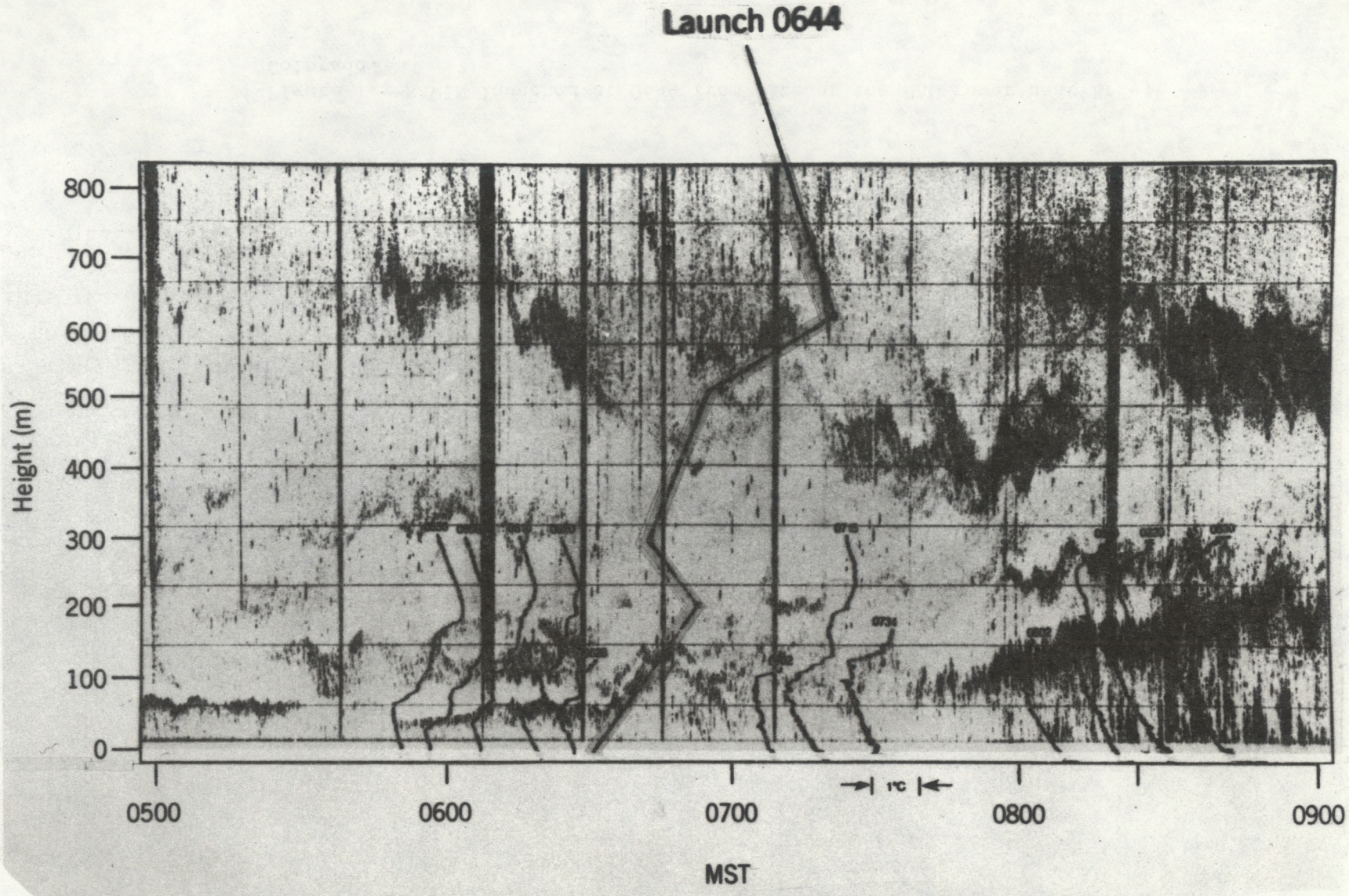

Figure 2.--Acoustic sounder record recorded at a site about 550 m from the BAO tower. Fast response temperature profiles recorded on a carriage traversing the tower are superimposed on the acoustic record. Note very good correlation between the temperature finestructure and the echo. Note herringbone structure of echoes indicating breaking KH waves.

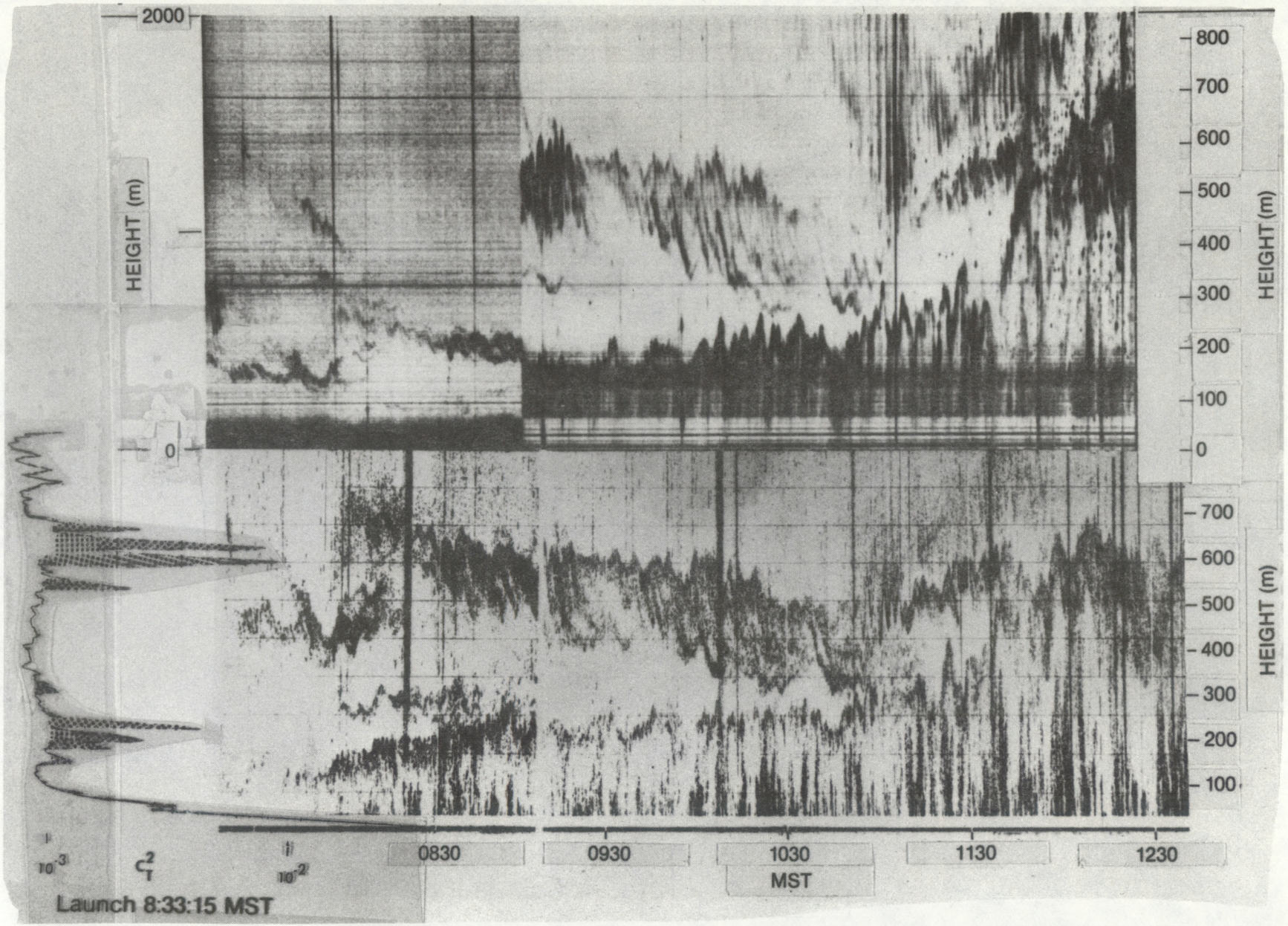

Figure 3.--Extension of the record of Fig. 2 with FM-CW radar record in top frame. The FM-CW height scale was reduced from 0-2000 m to 0-850 m to match the acoustic record at 0845 MST. A balloon-borne C_T^2 sensor (Ochs and Lawrence, 1972) was launched at 0833:15 MST and the C_T^2 profile is shown at the left of the acoustic record.

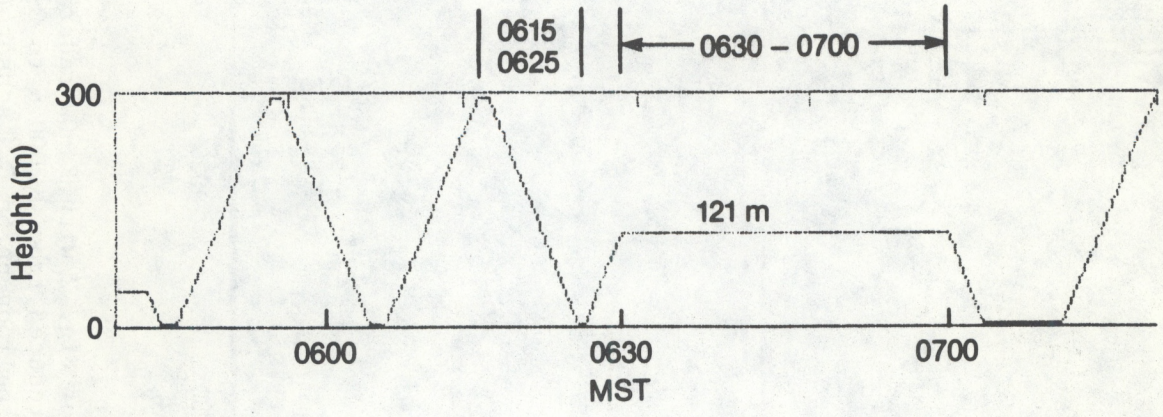

Figure 4.--Sample of carriage traverses and fixed level operation.

Lawrence (1972). This device consisted of two platinum wire sensors separated horizontally by one meter. The response frequencies of the platinum wires, the sonic wind sensors and the C_T^2 sensor exceeded 10 Hz and raw data were recorded at this rate. Although its response is excellent, the accuracy of the platinum wire thermometer is poor; however the quartz thermometers have an absolute accuracy of ±0.05°C and matched pairs were chosen for the booms.

An acoustic sounder and an FM-CW radar operated fairly near the tower pointing vertically. The sounders were about 550 m south of the tower to avoid serious tower clutter.

FINE STRUCTURE OF STABLE LAYERS REVEALED BY TOWER CARRIAGE TRAVERSES

Since the pioneering observations of Woods (1968) that revealed step-like profiles of temperature in the ocean's thermocline many observations of "sheet and layer" structures have been found both in salinity and temperature in estuaries, lakes and stably stratified zones in the oceans [e.g., Posmentier and Rachlin (1976), Molcard and Williams (1975), Gregg (1982)]. Such observations have not been reported (or have been poorly documented) in the atmosphere because, for the usual rates of ascent of balloons and aircraft, the response of the temperature and humidity sensors used has been inadequate to resolve very thin structures. However, the experiment described here used sensors whose response was better than 10 Hz and data digitized at 10 samples s^{-1}. The carriage rates of ascent and descent were 0.56 ms^{-1} and 0.58 ms^{-1} respectively. Thus 12 cm structures were resolvable in the Nyquist sense.

The temperature and wind profiles between 0616 and 0625, as revealed by the fixed-level sensors (generally 50 m apart), are shown in Fig. 5. However,

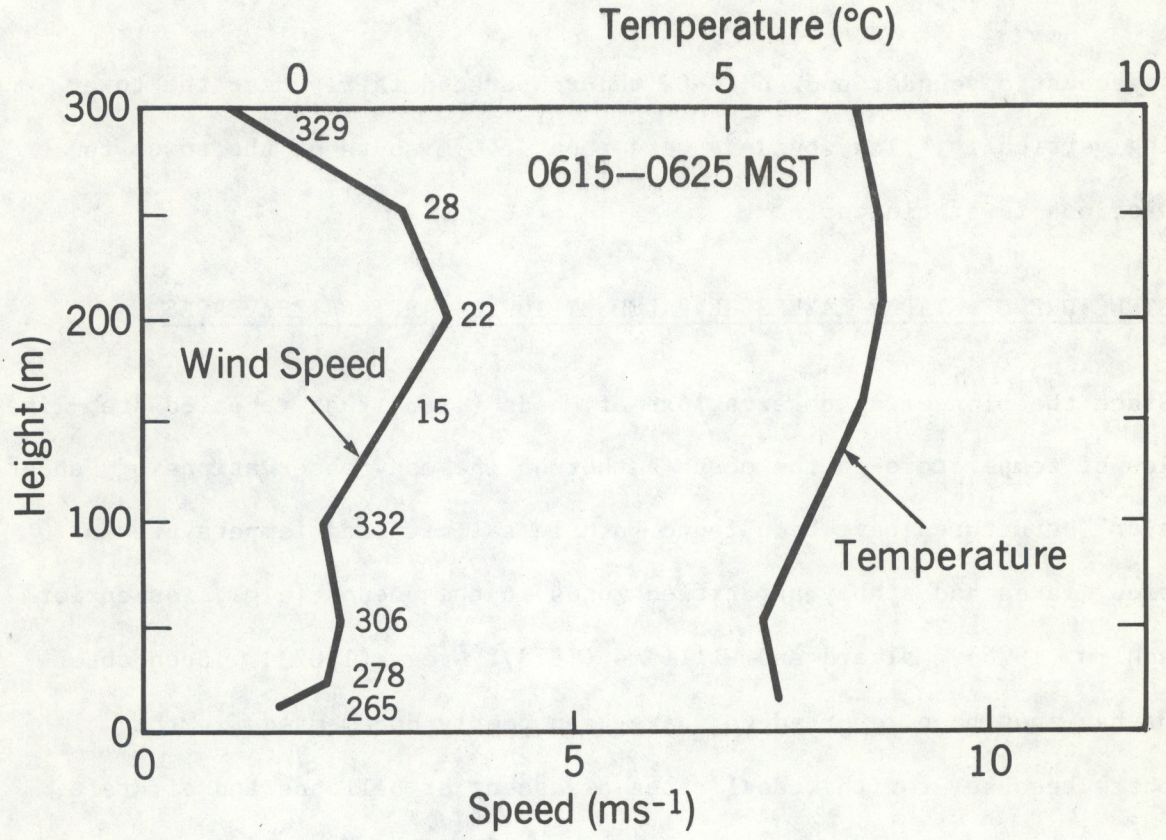

Figure 5.--Mean profile between 0615-0625 as recorded by the fixed-level sensors at 10, 22, 50, 100, 150, 200, 250 and 300 m levels on the tower.

fine structure profiles were obtained about every 10 min by carriage ascents and descents; each traverse took about 8.5 minutes. The resulting temperature profiles are shown superimposed on the acoustic sounder record in Fig. 2. A pronounced step structure is seen that is closely correlated with the acoustic backscattered power. The profiles are labeled with the time of the approximate midpoint of the ascent or descent. The step structure is especially evident in the profile labeled 0620 in which at least 4 sheets and layers are readily seen. More detailed profiles of temperature, along with sonic wind component profiles (parallel and perpendicular to the carriage boom) are shown in Fig. 6, 7, 8 and 9. Figures 7 and 8 include both boom temperatures. We see that the discontinuities are present in the velocity components as well as in temperature and that they are almost duplicated by the 2nd boom about 18 s later. For a wind speed of 2 ms^{-1} this implies good horizontal coherence of the thin layers over at least 36 m. Clearly the 50 m separation of samples in Fig. 5 produces a grossly simplified picture of the inversion structure. At 0644 MST a RAWIN was launched near the tower and the temperature profile from this launch is shown superimposed on Fig. 2. It substantiates the close relationship between echo intensity, wind shear and layers of large $d\theta/dz$ at heights higher than the 300 m tower. There is even some evidence in Fig. 1 for a layered structure within the tropopause. At 0833 MST a balloon-borne C_T^2 sensor was launched and the resulting profile is shown with the acoustic record in Fig. 3. It demonstrates the close correlation between C_T^2 and the echo layers. Ironically, although the radar-acoustic sounding systems tend to give the correct picture including fine structure, the deceptively smooth profiles given by conventional RAWIN's or aircraft are probably what are wanted for most meteorological applications. More will be said of this later.

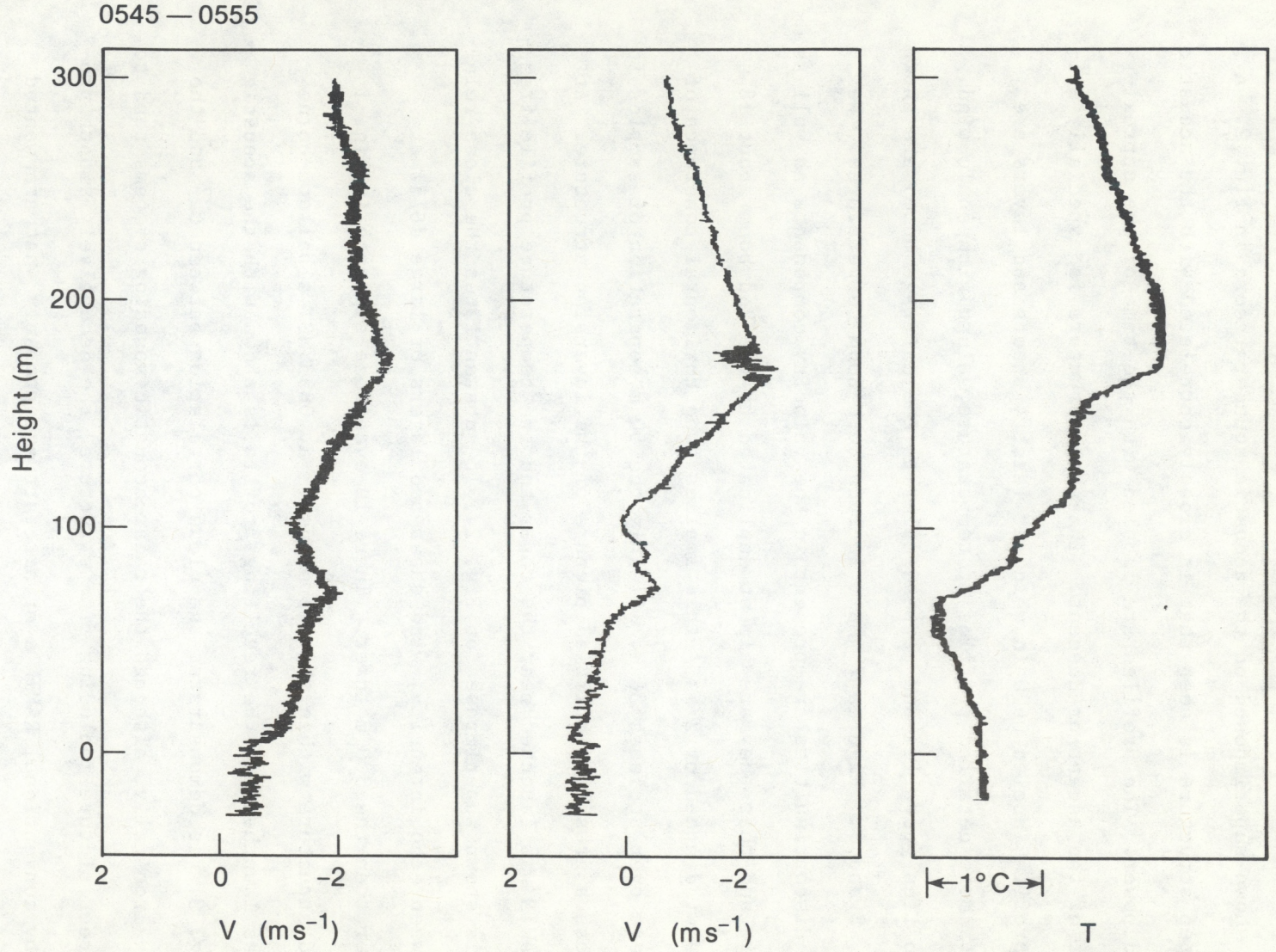

Figure 6.--Temperature and wind component measurements made during a carriage traverse during the time interval indicated (see Fig. 4).

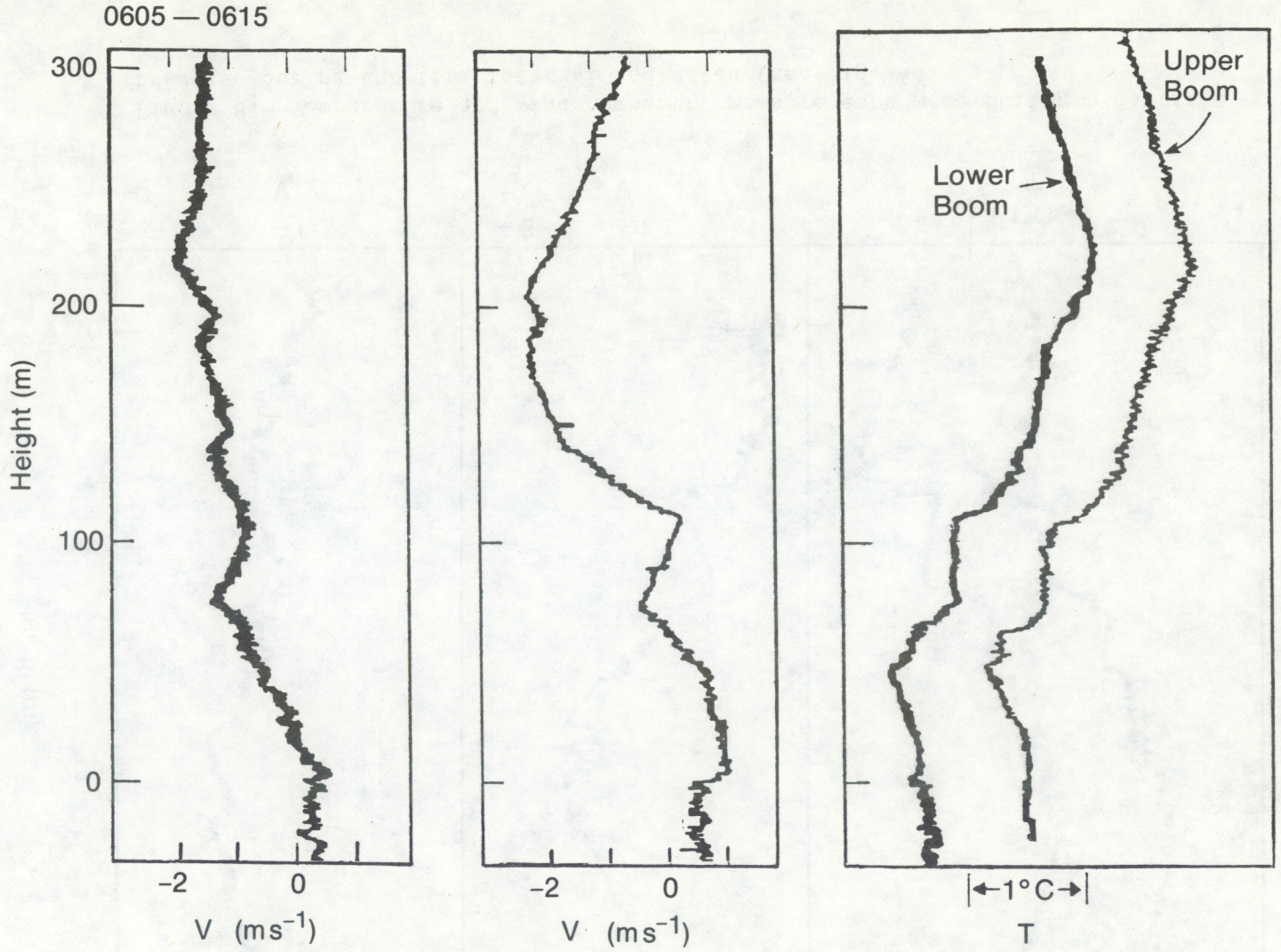

Figure 7.--Temperature and wind component measurements made during a carriage traverse during the time interval indicated (see Fig. 4).

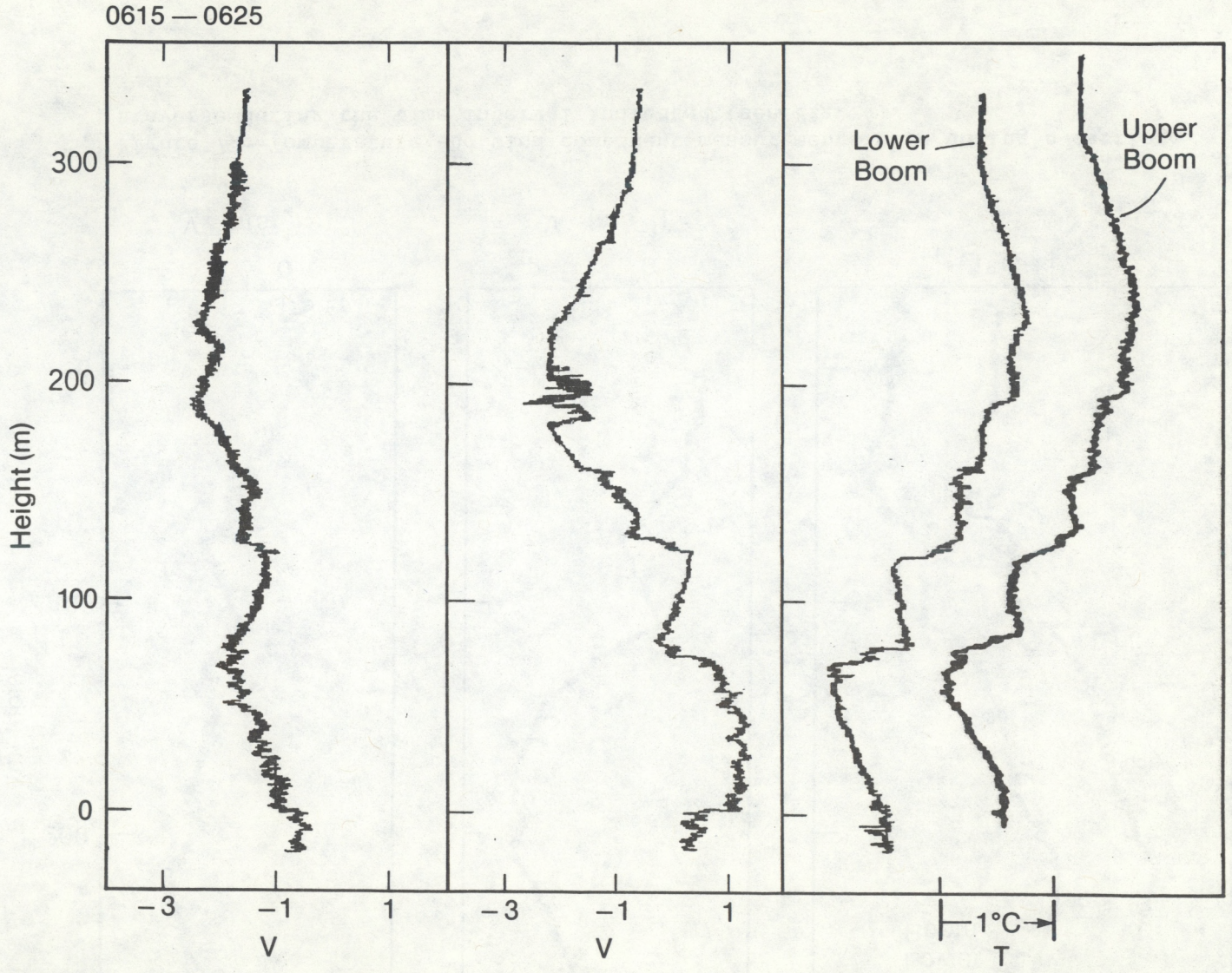

Figure 8.--Temperature and wind component measurements made during a carriage traverse during the time interval indicated (see Fig. 4).

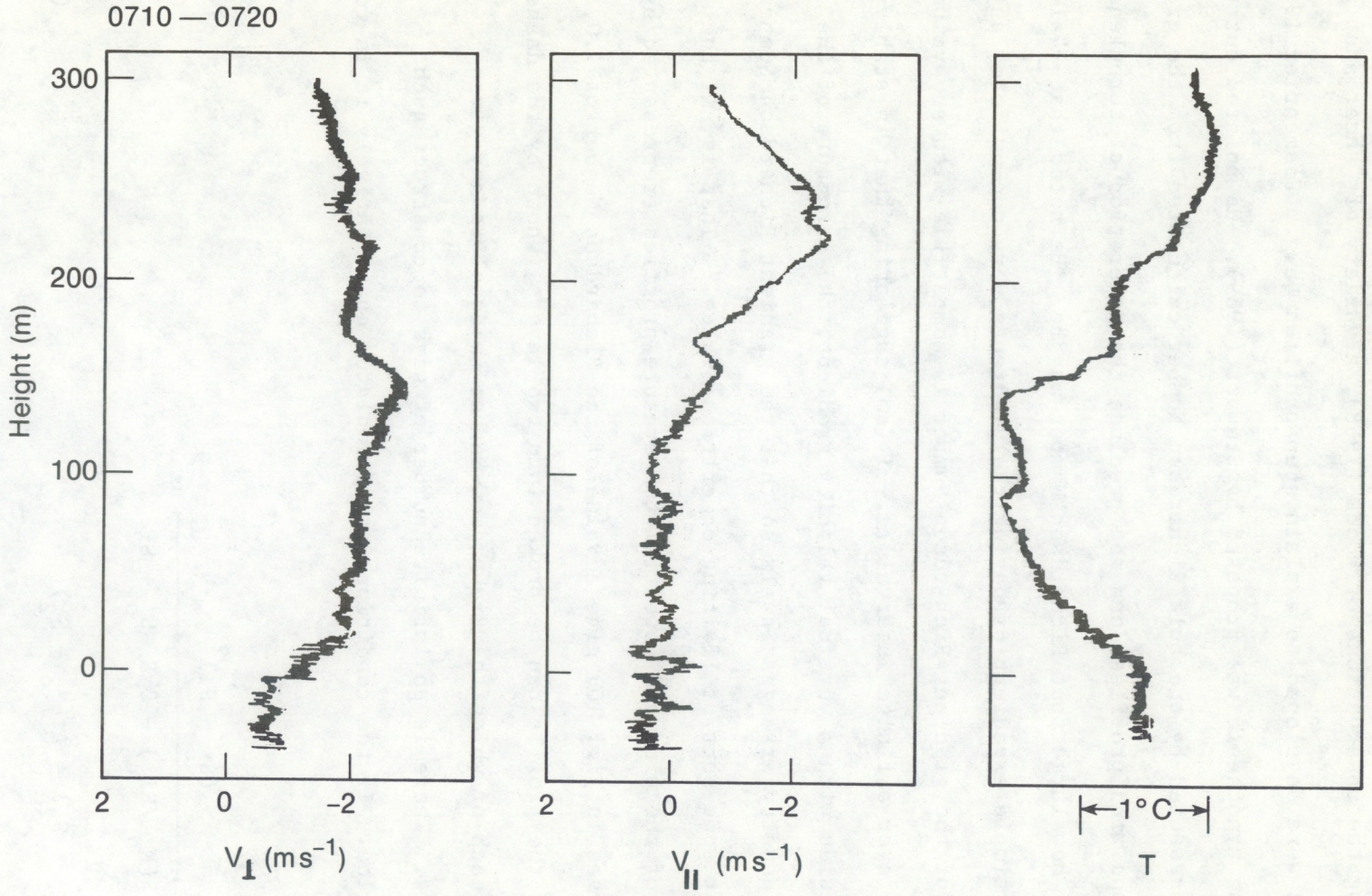

Figure 9.--Temperature and wind component measurements made during a carriage traverse during the time interval indicated (see Fig. 4).

SHEET AND LAYER FLUID MODELS

Following the observations of Woods (1968), a variety of "sheet and layer" models were developed to explain step profiles (e.g., Posmentier 1977). An interesting hypothesis was proposed by Stewart (1969). He pointed out that stability represented by the bulk Richardson Number calculated from the gross temperature and wind profiles does not preclude the generation of turbulence regardless of how large that Richardson Number may be. He noted that--"always, by the simple expedient of having the gradients very non-uniform, any value at all of the gradient Richardson Number is compatible with any value of $g(\Delta\rho\Delta z/\rho(\Delta u)^2$ over a finite interval Δz.--I (am) suggesting that in stably stratified fluids with a vertical velocity gradient, the structure of the velocity and density arranges itself so that the gradient Richardson Number is everywhere--at some sort of limiting or critical value." That is, if the gross values of the wind and potential temperature profiles (represented by the solid curves in Fig. 10) give a value of the Richardson Number of 1.0, a segment Δz of the profile can be broken into two layers, shown by the dashed profiles, in each of which the Richardson Number is equal to any given value--say 1/4. There is an infinite number of ways to construct such layered profiles. If the conditions are formulated quantitatively it is found that

$$h = \frac{(S_o - S_2)^2}{(N_o^2/Ri_c) - 2\,S_2\,S_o + S_2^2}\,\Delta z \qquad (1)$$

and

$$h(S_1 - S_2) = \Delta z(S_o - S_2) \qquad (2)$$

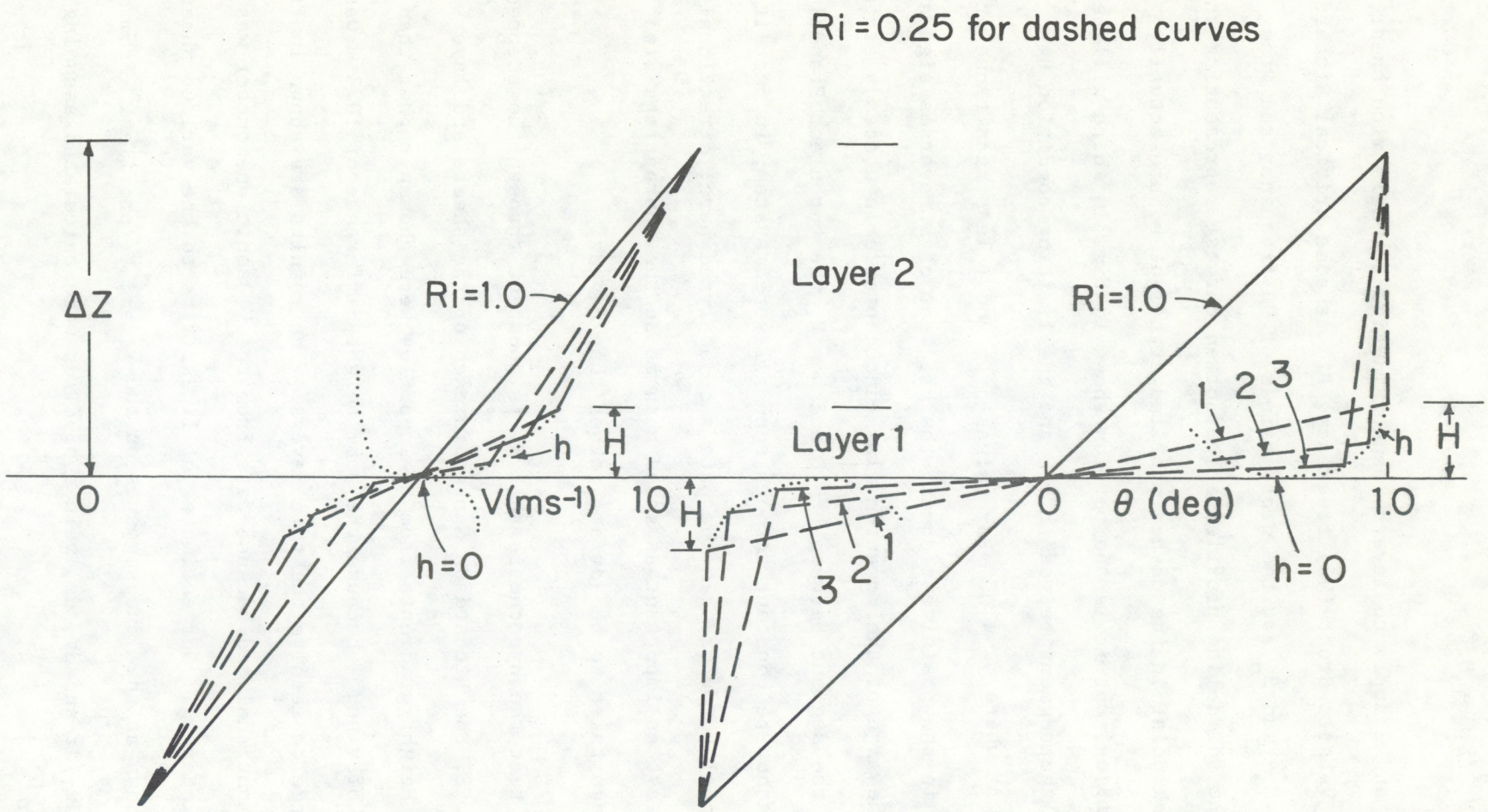

Figure 10.--Schematic picture of the way the finestructure of a stable layer, $2\Delta z$, can be chosen to make Ri = 1/4 even though the "bulk" structure of the layer (solid lines) gives a much greater value. The dashed curves are three such profiles out of an infinite number of possibilities all with the break-point, h, in the bi-linear profile lying on the dotted curve.

where $Ri_c = N_1^2/S_1^2 = N_2^2/S_2^2$.

The subscripts 1 and 2 apply to layers 1 and 2 in Fig. 10, S is wind shear, du/dz, N^2 is the Vaisala-Brunt (VB) frequency, Ri_c is some critical Richardson Number, say 1/4, N_o^2 and S_o are the gross values of VB frequency and wind shear based on the solid-line profiles. The dotted curves, representing the locus of the break-point in the dashed profiles at height h, are actually closed quasi ellipses, but it is the portion shown in Fig. 10 which will be discussed, i.e., the segment between h = 0 and the limiting condition h = $H = [Ri_c\ S_o/N_o^2]\ \Delta z$ where $S_2 \to 0$. For values of v and θ less than those at the h = 0 point, in the positive z domain the gradient of v reverses sign at h thus reversing the sign of the momentum flux--unacceptable in a steady state model. Even for the segment between h = 0 and h = H, the turbulent Prandtl Number, K_m/K_H, cannot be constant through such a layered system; in fact it must be proportional to dv/dz. In the data sets analyzed here, directional changes are at least as important as speed changes so the appropriate wind gradients have been taken to be $|d\underset{\sim}{v}/dz|$ rather than $d|\underset{\sim}{v}|dz$.

In order to test the hypothesis that Ri is constant through the stepped structure in Fig. 8, the Richardson Number in each of the sheets and layers was calculated. Height gradients from the profiles were chosen rather than boom differences of $\underset{\sim}{v}$ and T because the boom height difference of 10.3 m was sometimes too large to resolve the thin layers. The results are shown in Fig. 11. Layer 8 was not analyzed because data from the $V_\parallel$ sonic anemometer was bad during that interval. Our estimates of linear fits to the various sheets and layers are shown as the line segments on the $V_\perp$ and $V_\parallel$ profiles. From these values of $dv_\perp/dz$ and $dV_\parallel/dz$, values of dT/dz were calculated assuming

critical values of $Ri_c = 0.2$ and $Ri_c = 0.3$. The stippled sectors represent the range of differences in $d\theta/dz$ for these two values. (The larger gradient represents $Ri_c = 0.2$.) This procedure was used to provide not only an estimate of Ri within each sheet and layer, but also to indicate the sensitivity of the gradients and the profile of θ to fluctuations in Ri and in its critical value if such exists. The right-hand frame shows the corresponding profiles of T for Ri = 0.2 (solid) and 0.3 (dashed) that would be calculated from the wind profile data by integrating the temperature gradient data.

In spite of a degree of subjectivity in deciding what the thickness of some of the sheets should be and whether the sheets themselves should sometimes be split, as in zone 2 for example, we believe this data set provides convincing evidence supporting a critical value of Richardson Number between 0.2 and 0.3 throughout the stable region during this time interval, and we suggest, as Stewart proposed, that, as stratification proceeds, the profile tries to adjust itself toward a critical or saturation value of Richardson Number that just maintains turbulence to sustain the needed downward heat flux. The general agreement of the stippled sectors with the observed gradients indicates this value to lie between 0.2 and 0.3.

The sensitivity of the integrated-gradient profiles to small deviations in Ri and to small errors in the estimates of wind gradients in thin zones where the gradients are large leads to the conclusion that radar and acoustic wind data will not be able to provide accurate temperature profiles even though the temperature gradient information they provide can be very good under saturation conditions based on the third frame of Fig. 11. The difficulty in profiling by integrating gradients would be even greater in profi-

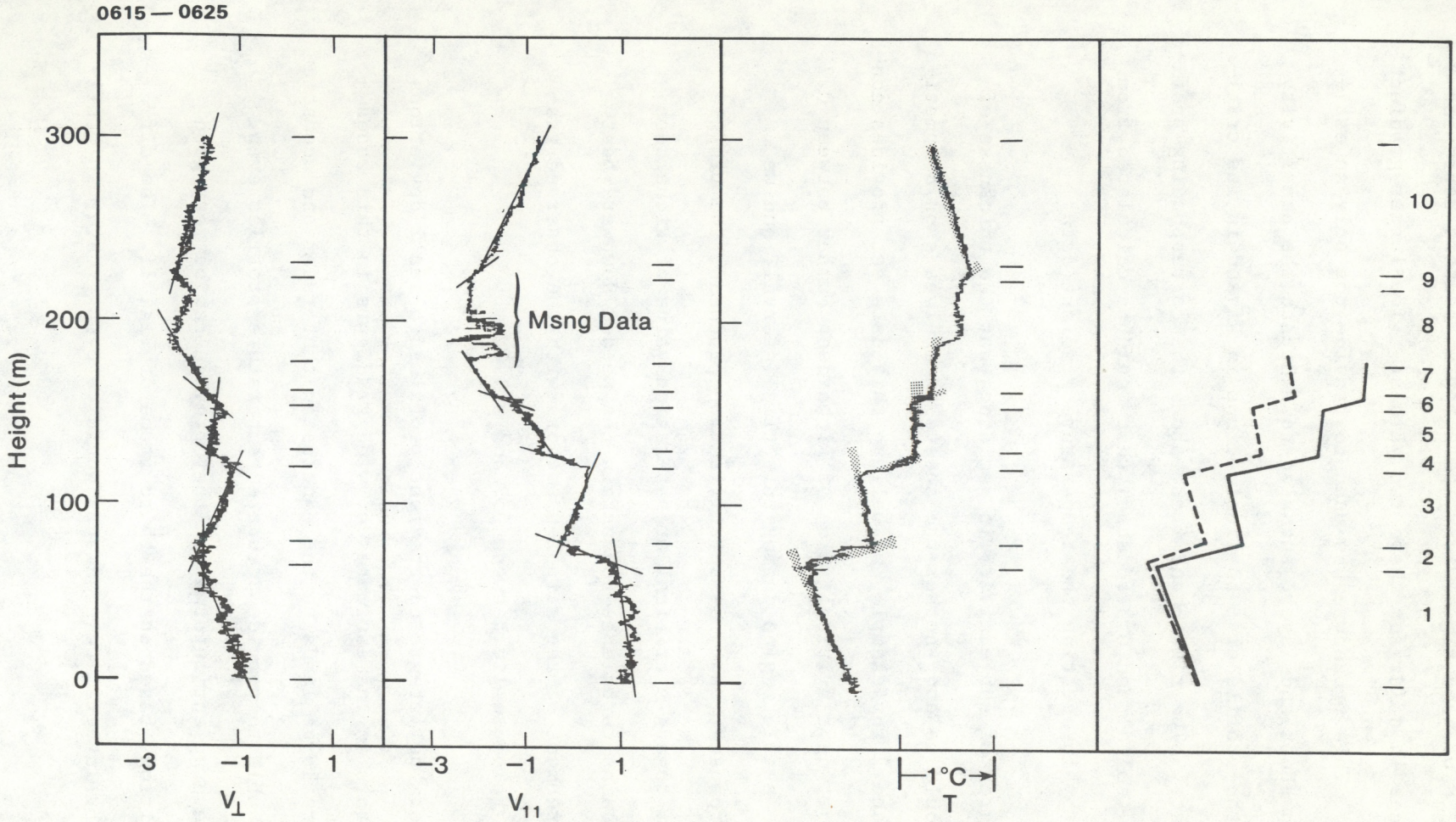

Figure 11.--Sonic anemometer wind profiles (components parallel and perpendicular to the carriage boom) and platinum wire temperature profile. Straight line segments on the wind profiles show gradients used to estimate temperature gradients from assumed values of the Richardson Number. The lower and upper bounds of the stippled sectors on the temperature profile are the temperature gradients calculated by assuming Ri = 0.2 and 0.3 respectively. The generally close correspondence between the stippled sectors and the observed profile gradients, indicates a Ri between 0.2 and 0.3 throughout the stable region of the profile. The Richardson Numbers calculated using the observed temperature profile are shown in Fig. 12.

les with less well defined layer structures. Even for the well layered structure in the descent from 0616-0614.5, without pre-knowledge of the temperature profiles, we would probably not have chosen layers at 6 and 9, for example. One solution might be to combine the radar information about layer gradients of temperature with radiometrically measured mean temperature profiles.

The carriage ascent from 0606 to 0614.5 does not show Richardson Numbers as low as those in the profile from 0616 - 0624.5 especially in the layers between steps (see Fig. 12) and in the layer of very weak turbulence between 77 and 110 m. This suggests that full saturation of the profile may be reached only as a limiting, steady state condition, and it remains to be determined how often the atmosphere proceeds to full saturation. Note the increased echo in Fig. 2 near the time of the 0620 sounding and the stronger velocity and temperature difference fluctuations shown in Fig. 12. In Fig. 12 $V_{\parallel}(t) - V_{\parallel}(t+0.9\ s)$ has been plotted because large spikes in the sonic anemometer record (deleted in the figure) precluded calculation of the structure function or structure parameter.

In summary these case studies support the conclusion that:

(a) There is a critical or saturation Richardson Number between 0.2 and 0.3 in elevated stable layers undergoing shear toward which profiles of wind and temperature tend. In stable layers with large radar or acoustic backscatter the Richardson number has reached its critical value of about 0.25.

(b) Radar and acoustic systems can provide useful and accurate gradients of temperature in elevated stable layers with strong backscatter if they can

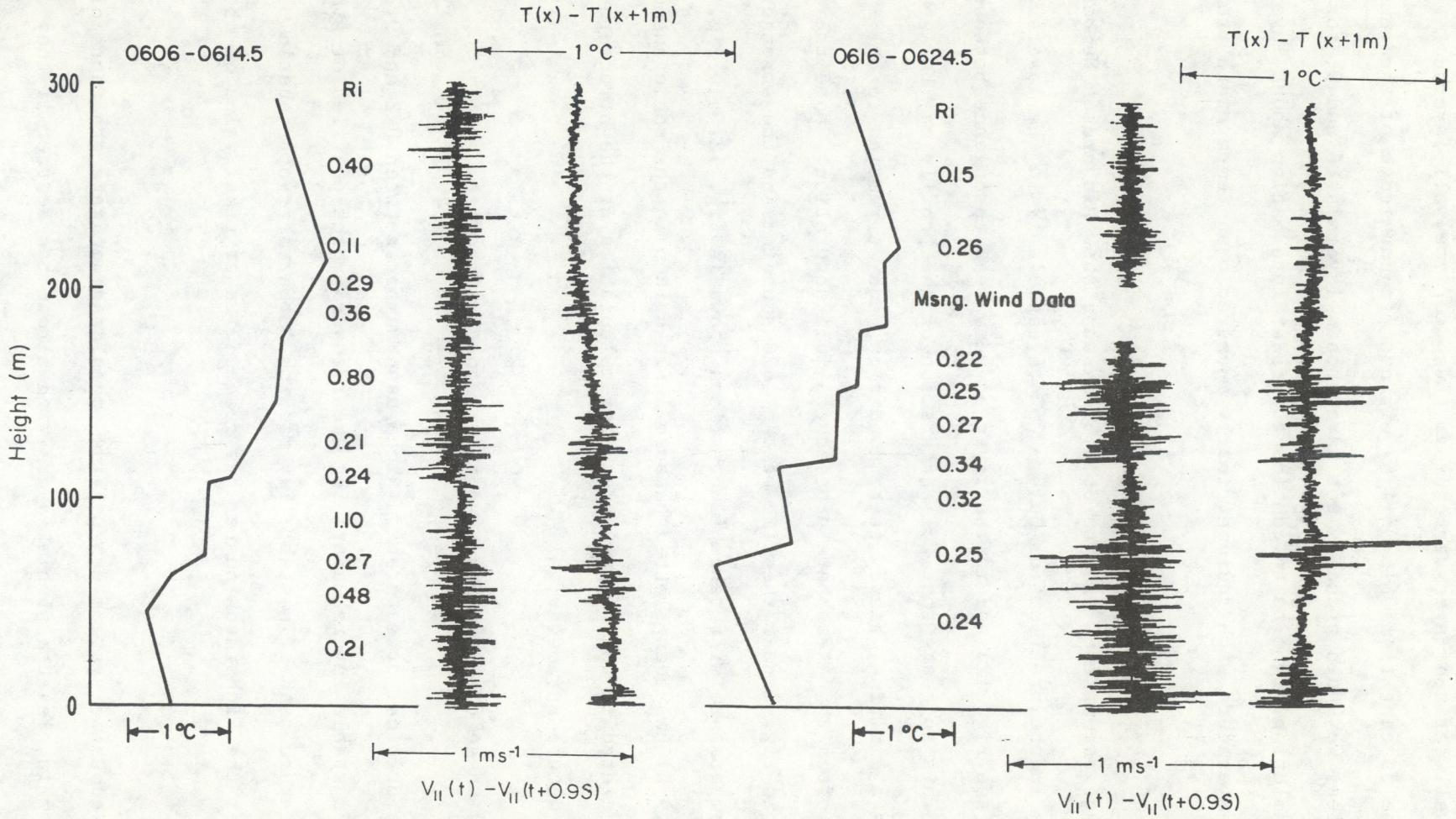

Figure 12.--Line segment temperature profiles with the corresponding Ri for the segmented zones during the carriage ascent from 0606-0614.5 and the carriage descent from 0616-0624.5. Raw differences of T' with 1 m horizontal separation and $u_{\parallel}'$ with 0.9 s lag are also shown.

be designed to provide accurate wind gradients with sufficiently high resolution. A large power-aperture product would be needed to sense the important frontal and subsidence inversions adequately at these resolutions.

(c) It does not seem practically possible to recover the bulk atmospheric temperature from gradient integration of the fine structure.

INITIATION OF A STEPPED PROFILE STRUCTURE

For the initiation of stepped profiles, such as those observed in these case studies, consider the sequence of events illustrated in Fig. 13. Suppose turbulence starts to die out in some layer (A) within a generally turbulent temperature inversion. Suppose the inversion zone had previously been essentially in steady state (constant heat flux indicated by heavy arrows). As the turbulence dies out, the heat and momentum fluxes decrease at the layer, leading to convergence above and divergence below, as shown schematically in Fig. 13. Therefore temperature rises above the layer and falls below. Similarly, if momentum flux across the non-turbulent layer ceases, the region above will decouple from the region below and velocity will increase above the layer and decrease below. However since the step in velocity is squared in the denominator of the Richardson Number, the Ri will be locally decreased as the process proceeds (dashed curves) until a critical value is reached (with profiles having steps lying on the dotted curves of Fig. 10) where turbulence is just maintained.

Figures 2 and 3 show almost ubiquitous Kelvin-Helmholtz waves throughout the time period in some of the layers, and it is logical to assume that the generation mechanism at the saturation Ri is KH waves.

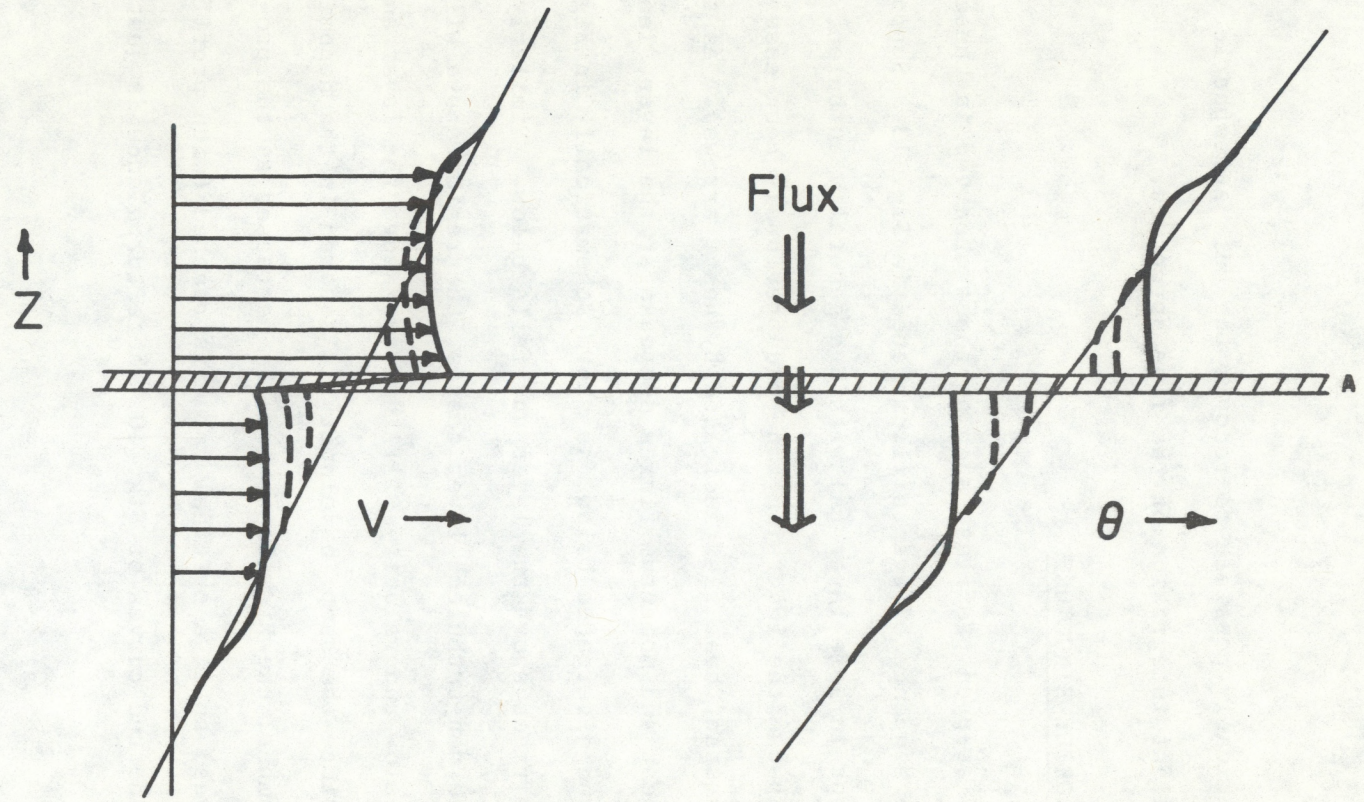

Figure 13.--Schematic picture of the way step profiles might be initiated from a formerly smooth, steady-state profile with constant downward flux of heat and momentum. In the hashed layer turbulence starts to die out causing convergence of heat above the layer and divergence below with resulting rise in temperature above the layer and falling temperature below as shown schematically for three successive stages by the dashed curves. Similarly, as the regions above and below the layer decouple, the wind above the layer speeds up and that below falls thus decreasing the Ri until turbulence is again initiated. Compare with Fig. 8.

THE KELVIN-HELMHOLTZ WAVE EVENT FROM 0610 to 0620

There is a clear wave event appearing as a braided structure on the acoustic sounder record between 100 and 140 m from 0610 to 0620. Figure 14 shows the temperature records (top three) and vertical velocity records (bottom three) at the 50, 100, and 150 m levels plotted from 10 second-averaged data. The wave event is clear at the 100 m level, but it is almost totally absent from the records at 50 and 150 m, although another wave event is present in vertical velocity at the 50 m level somewhat later. The path of the carriage is indicated by the straight lines in Fig. 14, and the 100 m level wave event occurs between the passage of the carriage up and down the tower. Fluctuations of the three velocity components and temperature are shown in Fig. 16. The sonic anemometers were used to measure the u, v, w components and the platinum wire sensor was used for temperature. The locus of the velocity vector fluctuations during the event is shown in Fig. 16 plotted in orthogonal planes beneath each wave for the time intervals between the vertical line segments on the plot of vertical velocity in the top frame. Figure 17 shows the plot of the vector wind in the horizontal plane through the whole event and shows the envelope of velocities lying between wave crests and troughs as well as the path of the changing mean wind vector as the event progressed.

The profiles measured during the carriage traverse from 0606 to 0615, before the wave event, are shown in Fig. 7. The profiles from the carriage descent at 0616-0625, after the event are shown in Fig. 8. It is seen that the wave event is located between 122 and 157 m and is undoubtedly associated with the shear in that region.

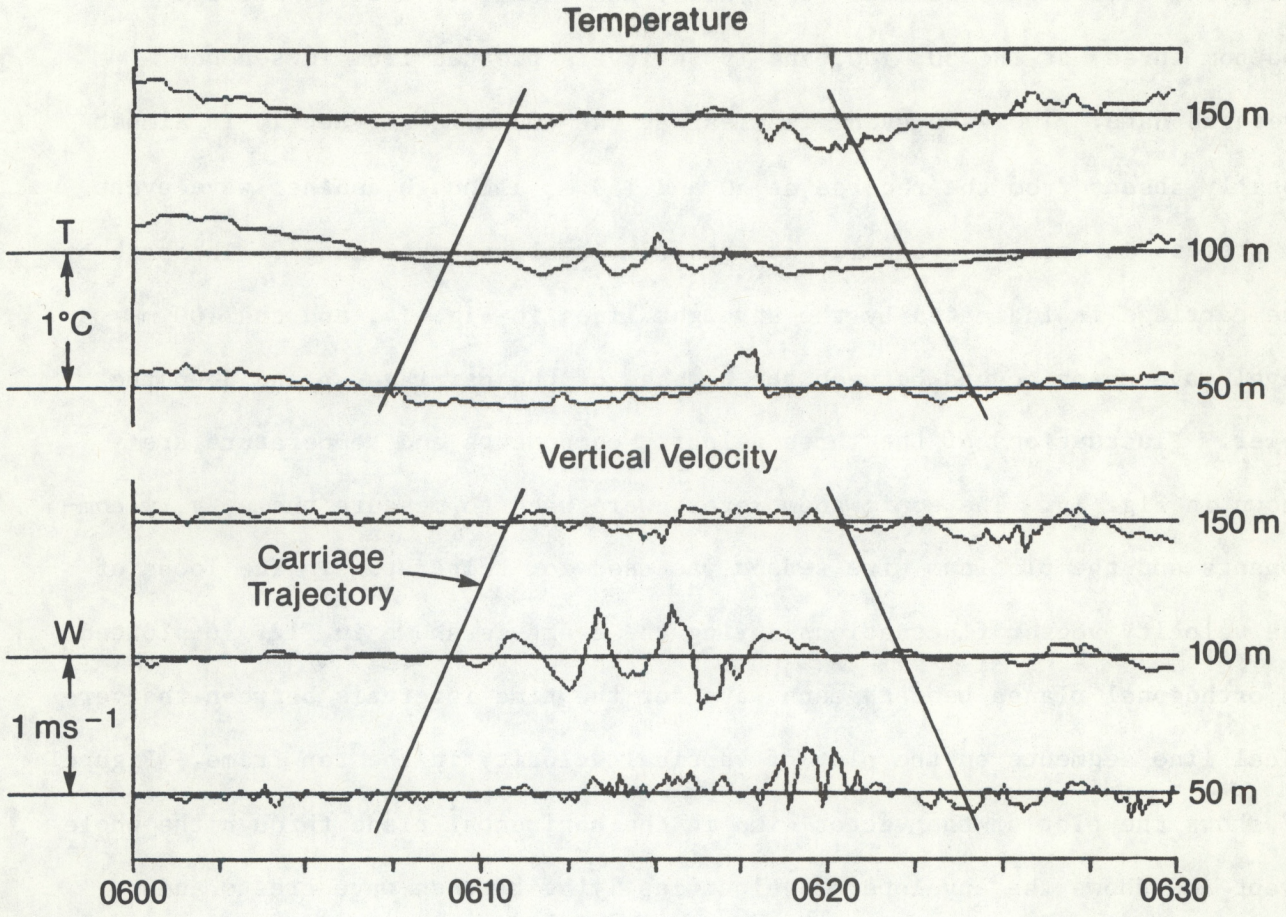

Figure 14.--Temperature and vertical velocity records at 3 fixed levels on the tower during passage of the KH wave event seen at 0610 in Fig. 2. The carriage traverses from 0606 to 0614.5 and 0616-0624.5 (straight lines) are seen to bracket the event.

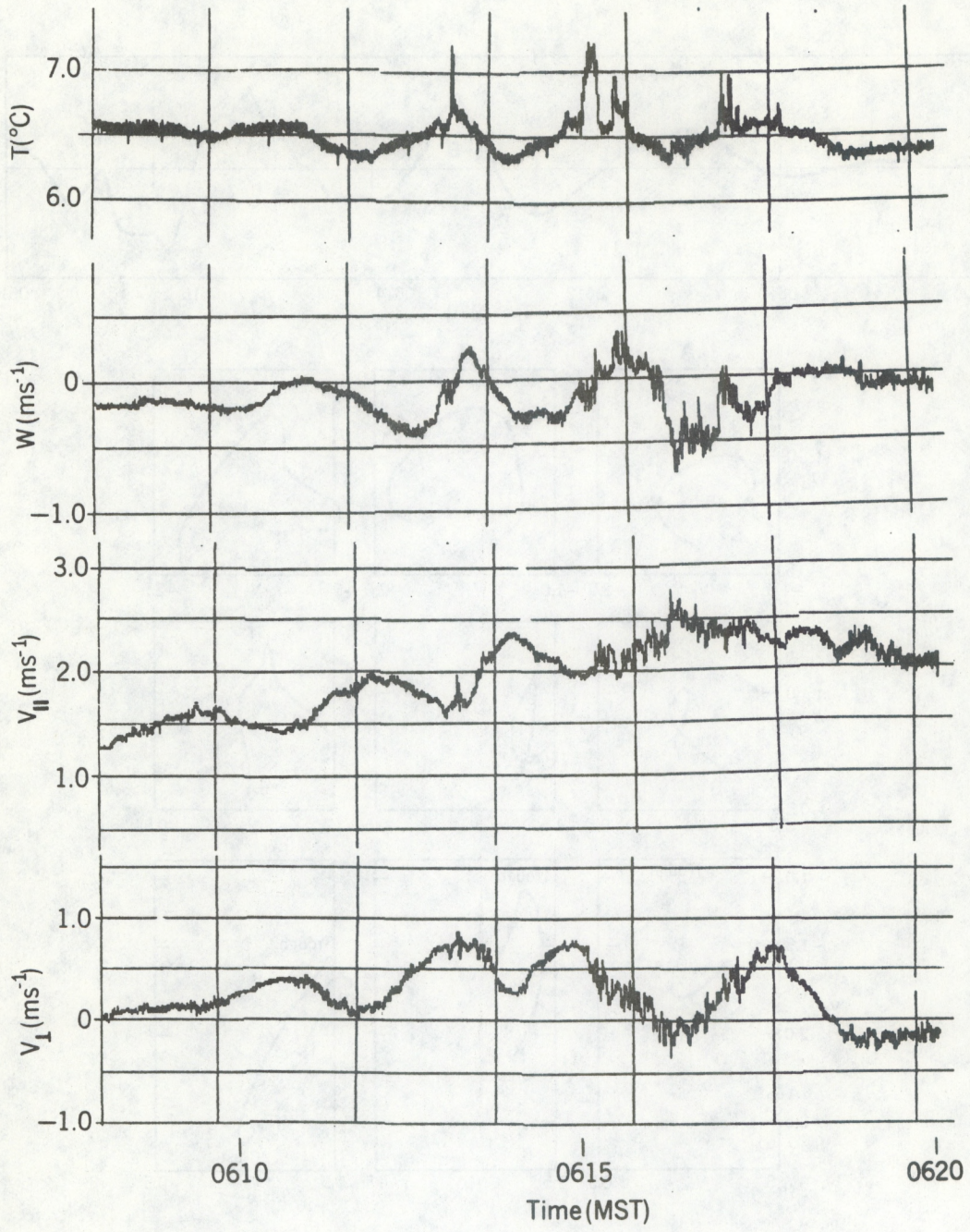

Figure 15.--The three sonic velocity components and platinum wire temperature at the 100 m level during the wave event. Note especially the sharp upward spikes in temperature that we believe result from displacement of sheet zone 4 down across the 100 m level by the waves.

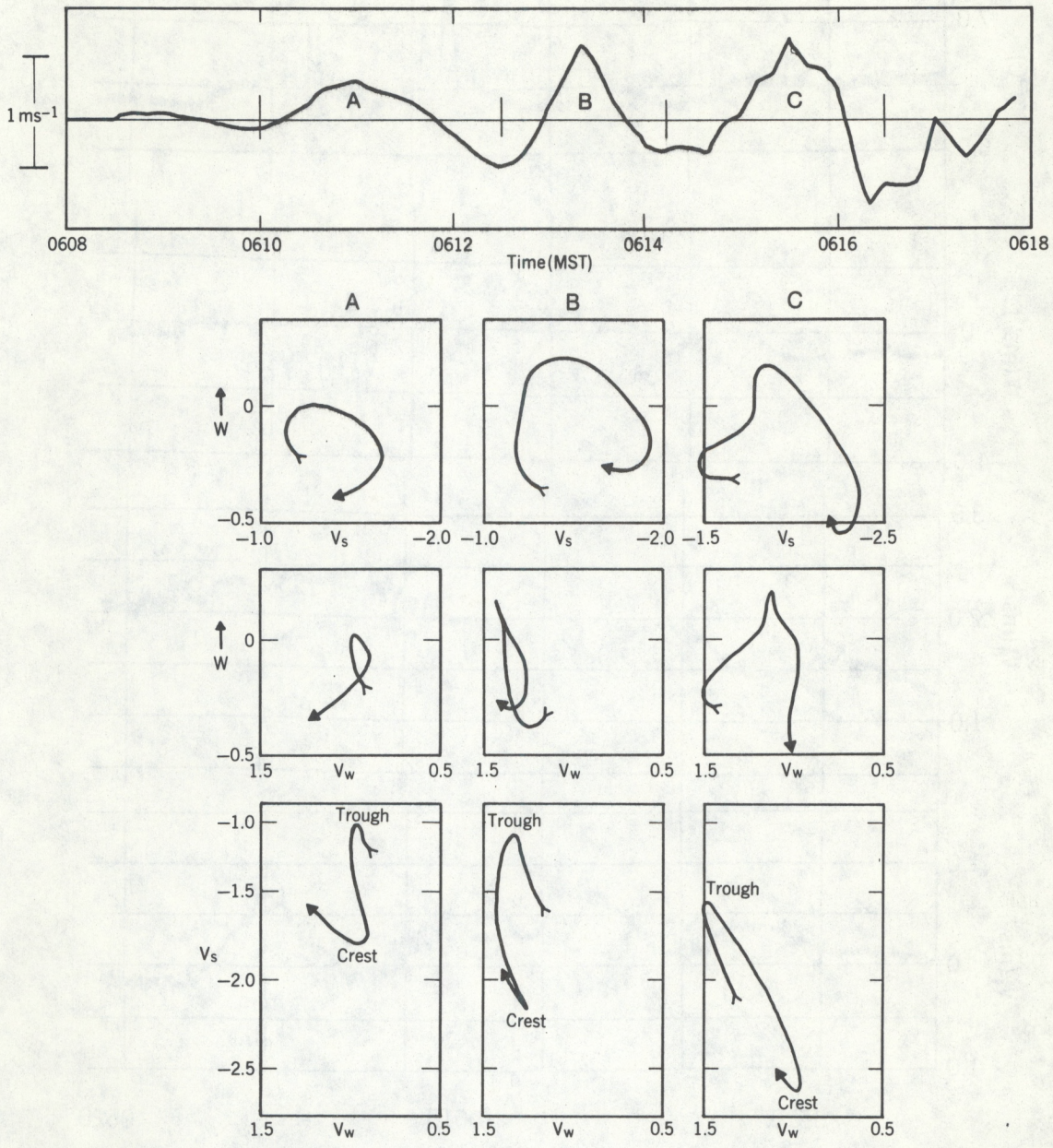

Figure 16.--The locus of the velocity vector fluctuations during the wave event of Fig. 16 projected onto three orthogonal planes beneath each wave for the time intervals between the vertical line segments on the plot of vertical velocity in the top frame.

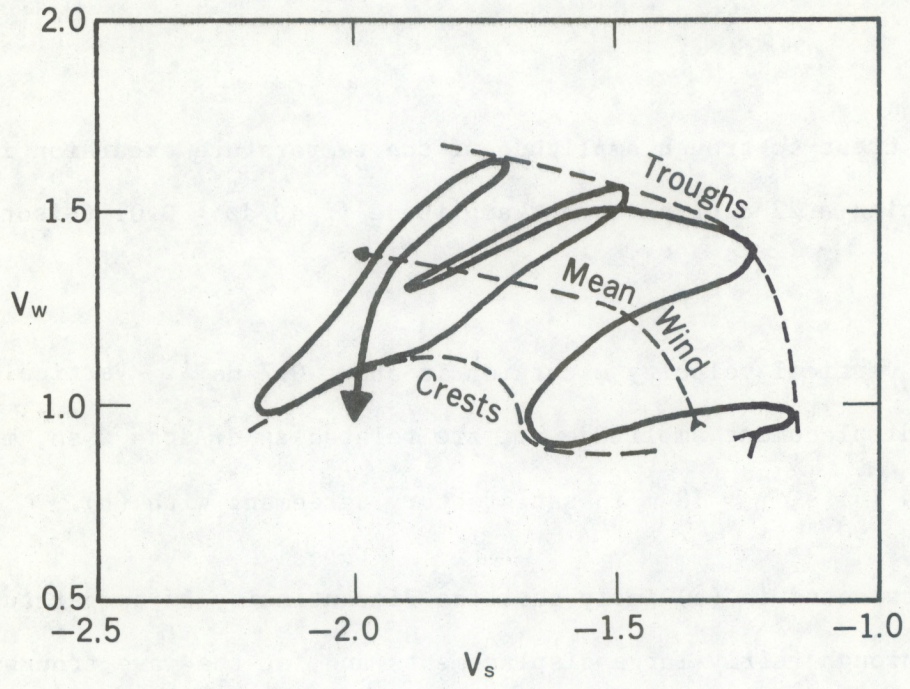

Figure 17.--Plot of the vector wind in the horizontal plane through the wave event. Shows the envelope of velocities lying between wave crests and troughs as well as the path of the changing mean wind vector at the 100 m level as the event progressed.

In attempting to place the waves relative to the profile discontinuity precisely, several observational facts should be noted:

(a) Sharp spikes in temperature are seen in Fig. 15 at the crests of the waves in temperature. (These crests correspond to downward displacement, because potential temperature is increasing with height.) These spikes are 0.6-0.7 C, which is about the magnitude of the temperature discontinuity at 120 m.

(b) The crest-to-trough amplitude of the temperature excursion is about 0.22°, suggesting a 22 m displacement amplitude if $d\theta/dz \simeq 0.01$ (~isothermal lapse rate).

(c) The vertical velocity excursion is about 0.7 ms^{-1}. Vertical velocity, w, and displacement amplitude, η, are related as $d\eta/dt = w$ so, if the wave period is 141 s, $\eta \simeq 18$ m in satisfactory agreement with (b).

The points noted in (a) imply that the discontinuity in temperature is being swept through fairly large displacements and, at the wave troughs, even occasionally gets below the measurement level at 100 m. This is in agreement with the dark region of the braided structure seen in the SODAR record. If this identification is made, the acoustic record shows the interface perturbation is 40-50 m.

The behavior noted in (b) implies that the 100 m level is in zone 3 of Fig. 11, below the interface at 4, nearly all the time. Together, (b) and (c) imply that the wave event diminishes rapidly below the interface; it is reduced to 1/2 amplitude a distance of 22 m below.

If the waves are at a critical level and thus are traveling with the mean wind speed at their height (say 1.7 ms^{-1}) their wavelength is 240 m. If a breaking wave is plotted to scale using this wavelength and an amplitude of 40 m (as suggested by the SODAR record) it appears as shown in Fig. 18. If the corresponding time scale is compressed by a factor of 20, the same wave appears as shown in the upper frame of Fig. 18 and bears a close resemblance to the wave train in the SODAR record. Figure 16 has been drawn to illustrate the various relationships noted above between the wave event and the layer interface. The solid curve represents the displacement of an isentrope in the breaking wave and the dashed curve the displacement perturbation at the 100 m level. A zone of convective mixing is shown schematically where the cooler air from below has been injected above warmer air by the breaking wave.

In summary, a KH wave event was initiated in zone 5 of Fig. 11 by the relatively large shear in that region. The "breaking" waves produced active turbulence and mixing in that zone as suggested by the decrease in potential temperature gradient and shear in $V_{\perp}$ seen in the profiles after the event (see Fig. 12). In fact the layer called zone 5 was ill defined before the event. In Fig. 12 the profiles $V_{\parallel}(t) - V_{\parallel}(t+\tau)$ are shown for the traverses before (left) and after (right) the event, and the increase in temperature fluctuation and velocity fluctuation in zone 5 after the wave event is large.

Even the wavelength and layer thickness are in good agreement with the most unstable wavelength based on the neutral curves in some classical models (see Gossard and Hooke, 1975). The models of Drazin (1958) and Holmboe (1960) give, respectively

$$\lambda/\Delta z \simeq 4.5, \qquad \lambda/\Delta z \simeq 6.3$$

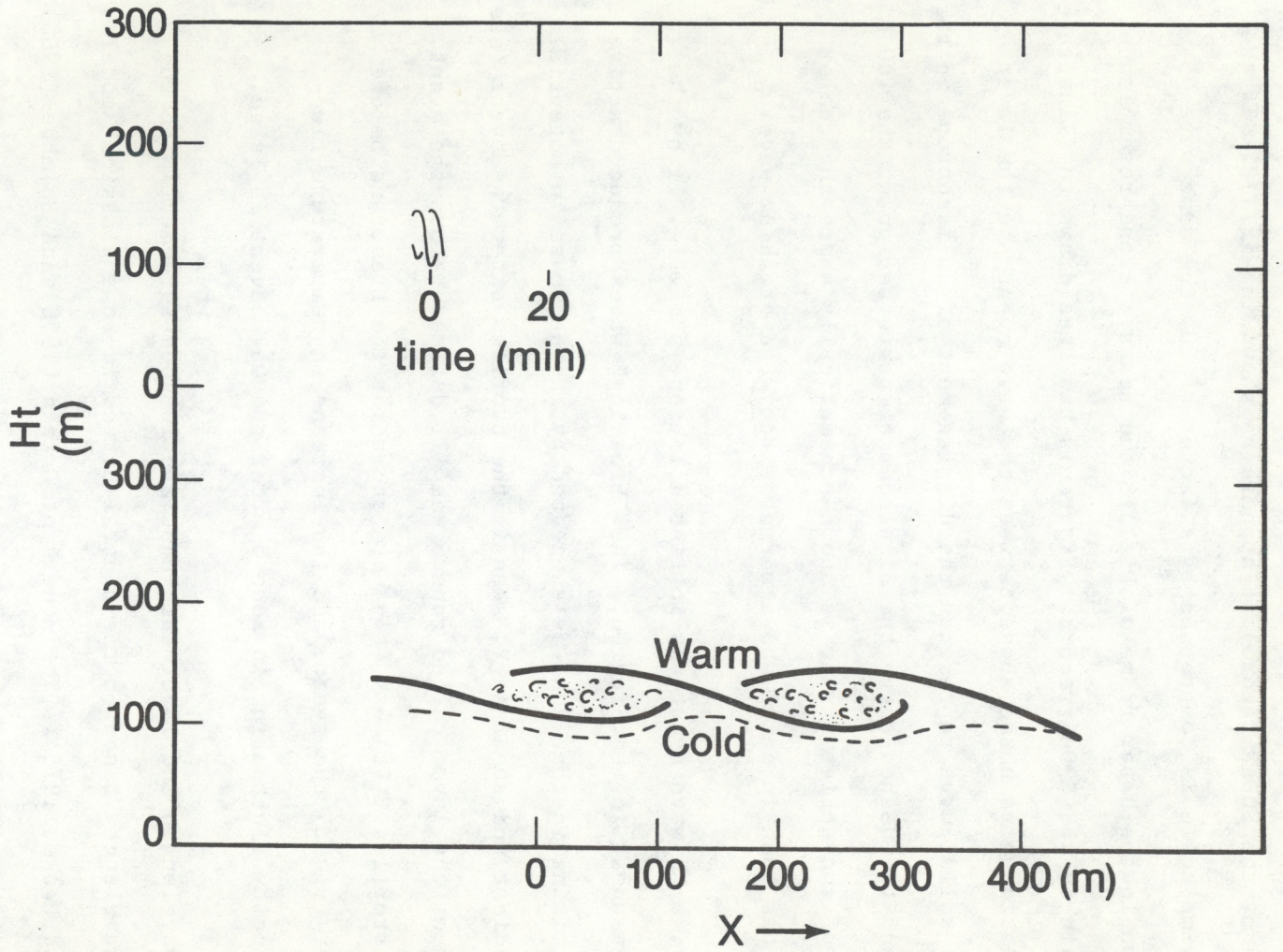

Figure 18.--How a wave whose spatial appearance is schematically shown in the lower frame, would appear on a very compressed time plot. Note resemblance to herring-bone structures in Fig. 2.

where the wavenumber k is $2\pi/\lambda$, λ is wavelength and Δz is the total layer thickness in their respective models. If the waves are presumed to travel with the mean wind speed at the center of the layer (say 1.7 ms^{-1} for layer 5) their wavelength is 240 m. If the layer is 35 m thick, $\lambda/\Delta z \simeq 6.8$ in good agreement with the Holmboe model.

Close examination of Fig. 2 shows "herring bone" structures like the top frame in Fig. 19 to be common throughout all the layers (except perhaps the lowest) in the figure, supporting the conclusion that turbulence is generated by shear-induced wave instability associated with a critical Richardson Number between 0.2 and 0.3.

The power spectra for temperature and vertical velocity for the 20-minute interval between 0605 and 0625 are shown in the top frame of Fig. 19. The cospectrum (heat flux spectrum) is shown in the bottom frame. The spectra show a well-defined peak at a wave period of 141 s. Range bars of 90% confidence in the spectral estimates are shown on the spectra. The flux of heat at the 100 m level is indicated to be strongly upward at the wave frequency and quite dominates the rest of the spectrum. The spectrum of phase lag between temperature and humidity is shown in Fig. 20. The indicated phase angle at the wave period is 289°. Therefore, temperature and vertical velocity are not precisely in quadrature, which explains the flux present at the wave frequency. The 90% confidence range in angle is 270-315°, which seems to imply that this puzzling result is real.

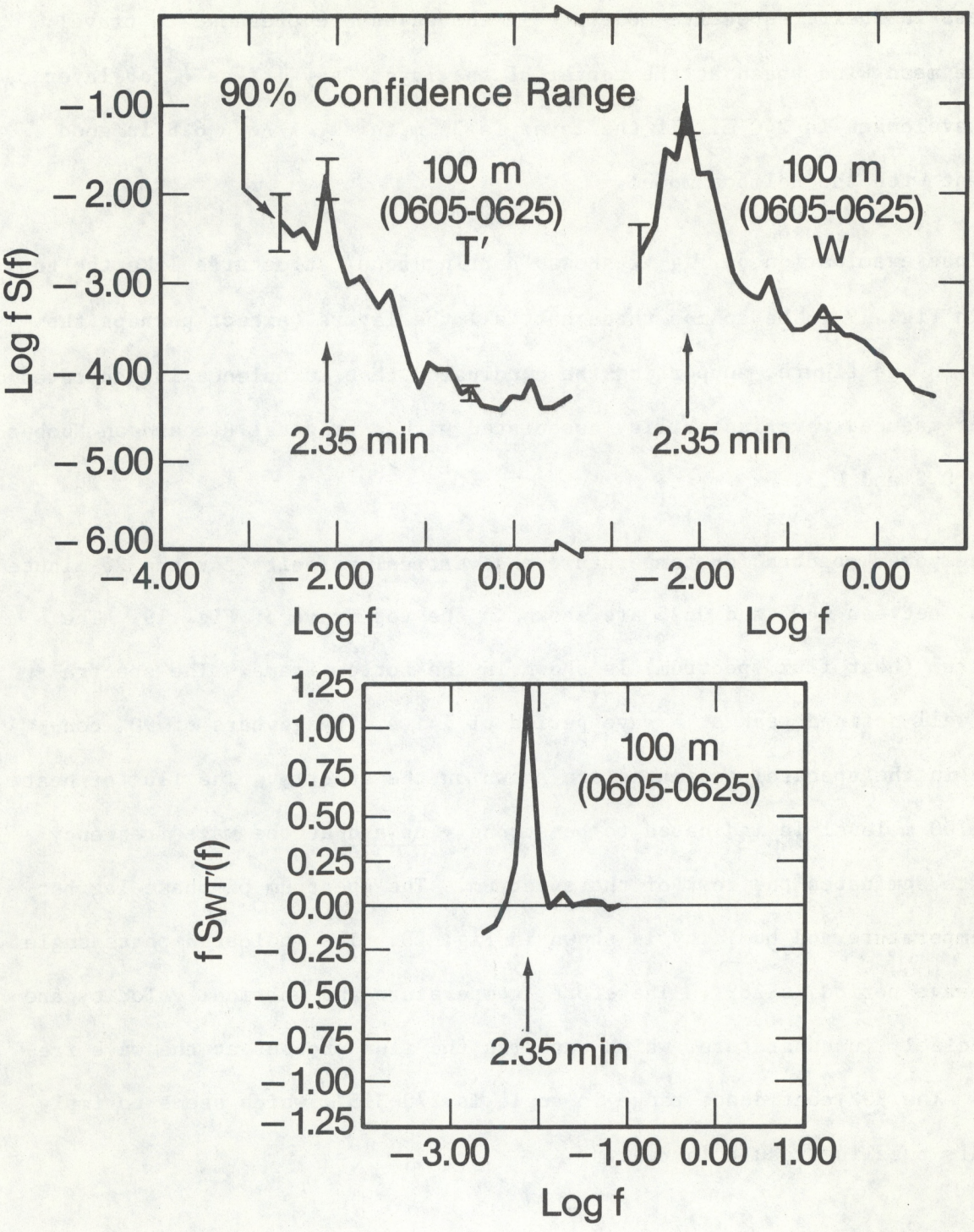

Figure 19.--Power spectra of vertical velocity and temperature (top frame) and their cospectrum (bottom frame) during the wave event.

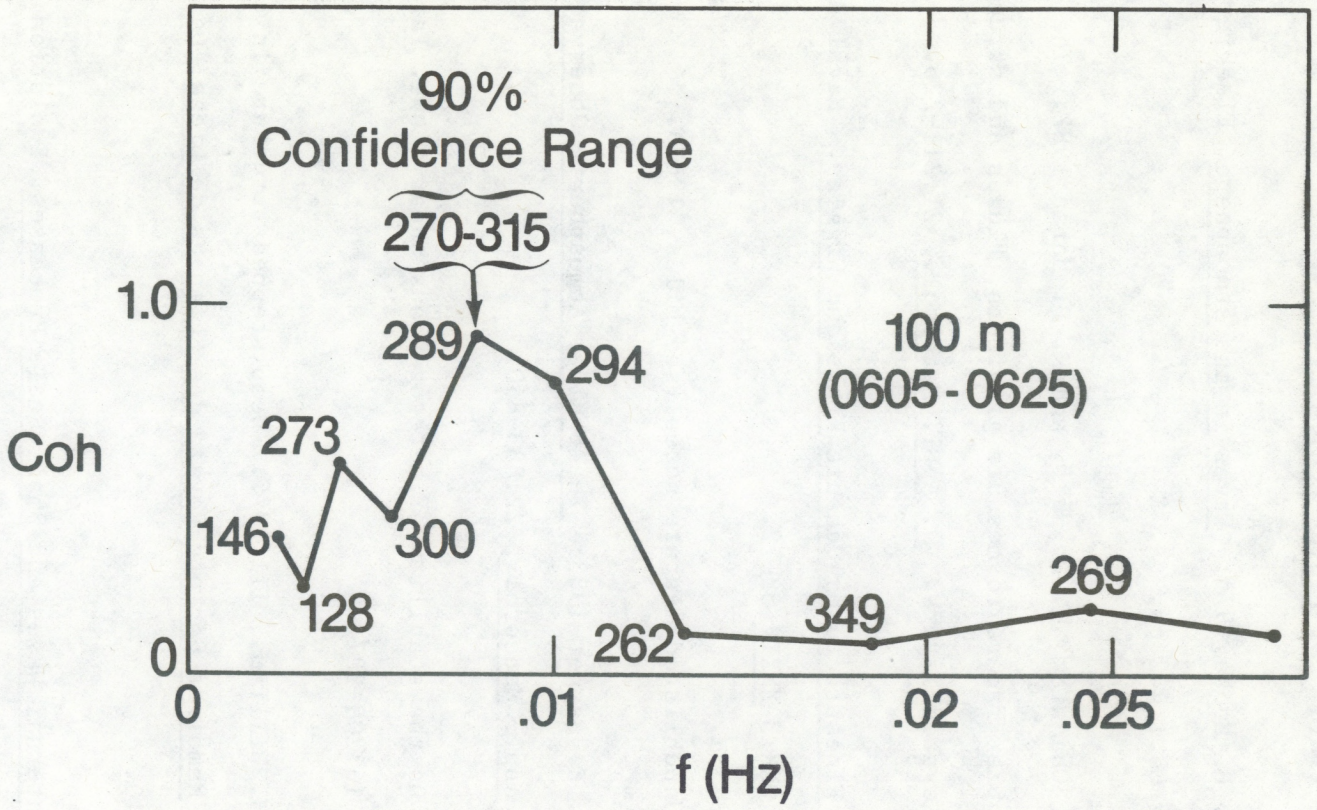

Figure 20.--Coherence between temperature and vertical velocity (solid curve) and the phase angle between them (numbers). The range of phase angle for 90% confidence (based on the co and quadrature spectra from which it is calculated) is shown for the point of maximum coherence. They are not precisely in phase quadrature leading to the spike of upward heat flux shown in Fig. 20.

REFERENCES

Drazin, P. G., 1958: The stability of a shear layer in an unbounded heterogeneous inviscid fluid. J. Fluid Mech. 4:214-224.

Gossard, E. E. and W. H. Hooke 1975: Waves in the Atmosphere, Elsevier Scientific Publishing Co., 442 pp.

Gossard, E. E., R. B. Chadwick, W. D. Neff, and K. P. Moran 1982: The use of ground-based Doppler radars to measure gradients, fluxes and structure parameters in elevated layers. J. Appl. Meteorol., 21:211-226.

Gregg, M. C., 1982: Finestructure: Oceanic Kinks and Wiggles. Naval Research Reviews, ONR 3 XXXIV 52-72.

Holmboe, J., 1960: Unpublished lecture notes (see Miles, 1963).

Kaimal, J. C., and J. E. Gaynor 1983: The Boulder Atmospheric Observatory, To appear in J. Appl. Meteorol., 22:883-860.

Miles, J. W., 1963: On the stability of heterogeneous shear flows. Part 2. J. Fluid Mech., 16:209-227.

Molcard, R., and A. J. Williams, III 1975: Deep stepped structure in the Tyrrhenian sea, Memoires Societe Royale des Sciences de Liege, 6e serie, tome VII, 191-210.

Munk, W. H. 1981: Internal Waves and Small Scale Processes, Evolution of Physical Oceanography, Scientific Surveys in Honor of Henry Stommel; B. A. Warren and C. Wunsch eds. MIT Press 264-291.

Ochs, G. R., and R. S. Lawrence 1972: Temperature and C_n^2 profiles measured over land and ocean to 3 km above the surface, NOAA TR ERL 251-WPL 22, 39 pp.

Posmentier, E. S. The Generation of Salinity Finestructure by Vertical Diffusion, J. Phys. Oceanog., 7:298-300.

Posmentier, E. S., and J. W. Rachlin 1976: Mixing of seawater and freshwater in the Hudson Estuary, J. Phys. Oceanog., 6:775-777.

Woods, J. D. 1968: Wave-induced shear instability in the summer thermocline, J. Fluid Mech., 32:791-800.